INTERNATIONAL JOURNAL FOR NUMERICAL METHODS IN FLUIDS
Int. J. Numer. Meth. Fluids 2007; **54**:805–830
Published online 7 February 2007 in Wiley InterScience (www.interscience.wiley.com). DOI: 10.1002/fld.1444

An adaptive control system using the fuzzy theory for transient multi-physics numerical simulations[‡]

Toshiharu Muramatsu[1] and Genki Yagawa[2,∗,†]

[1]*Japan Atomic Energy Agency, 4002, O-arai, Ibaraki 311-1393, Japan*
[2]*Toyo University, 2-36-5, Hakusan, Bunkyo-ku, Tokyo 112-8611, Japan*

SUMMARY

An adaptive control system to yield optimum time step sizes was developed using the fuzzy theory for transient multi-physics numerical simulations. Applications of the control system reveal considerable amount of the computing time savings, typically by 50–75% of the computing time required when the time step size was not controlled by the system. The result obtained in this work is very encouraging in the sense that the adaptive control system would be used as one of the efficient measures for saving computing time when one wishes to perform extremely large-scale computations in transient multi-physics numerical simulations. Copyright © 2007 John Wiley & Sons, Ltd.

Received 21 November 2006; Revised 10 December 2006; Accepted 11 December 2006

KEY WORDS: adaptive control; fuzzy theory; multi-physics numerical simulations

1. INTRODUCTION

Recent interests in thermohydraulic design and safety evaluations of liquid metal-cooled fast breeder reactor (LMFBR) or liquid metal reactor (LMR) have stimulated a need for highly accurate computations of relatively slow but turbulent flows in complicated flow geometries. Much attention is being focused on the decay heat removals due to the natural circulation capability of the sodium coolant system after reactor shutdown, in which the interactions of local and global phenomena in the presence of buoyancy forces result in producing significant departure from one-dimensional systematic behaviours. The design and safety evaluation of such a heat transport system require very accurate solutions of the entire three-dimensional transient flow and temperature fields.

[∗]Correspondence to: Genki Yagawa, Toyo University, 2-36-5, Hakusan, Bunkyo-ku, Tokyo 112-8611, Japan.
[†]E-mail: yagawa@eng.toyo.ac.jp
[‡]This was originally submitted as part of the ICFD SPECIAL ISSUE.

Accurate solutions of buoyancy dominated flows could be obtained using the class of algorithms referred to as higher-order difference schemes as opposed to the conventional first-order upwind scheme. In the use of such higher-order difference schemes as quadratic upstream interpolation for convective kinematics (QUICK) [1], however, two serious problems must be overcome: (i) numerical instability mainly as a result of non-physical wiggles, in particular when large time step sizes are employed and (ii) high computational cost as a result of small time step sizes required to ensure both stability and accuracy in time. In spite of the use of filtering remedy and methodology (FRAM) [2], which was developed to eliminate the non-physical wiggles, the time step size requirement is still not alleviated. Unfortunately the optimum time step sizes cannot be predetermined and vary from case to case.

The objective of the present work is to develop an adaptive time step size control system based on the fuzzy theory [3, 4] and to demonstrate overall improvement in the computing cost reduction for large-scale numerical simulations, where we focused on the elimination of numerical instability by the control system. For example, starting from unknown velocity and temperature distributions in the system of concern, we try to get the steady-state distributions with a minimum computing effort by carrying out a null-transient numerical simulation under the constant boundary conditions. Therefore, it is of interest to us how fast the simulation reaches a unique steady-state solution without numerical instabilities, no matter how different the course of simulations due to the differences in time step sizes used.

The adaptive control system to be discussed in the following fully utilizes the expertise accumulated in code users and numerical experts: e.g. the use of very small time step sizes is recommended when a symptom of instabilities appears, and relatively large time step sizes otherwise. This system was implemented into a single-phase multi-dimensional thermohydraulics code, AQUA [5], based on time-averaged Navier–Stokes equation and into a single-phase multi-dimensional thermohydraulics quasi-direct numerical simulation code, DINUS-3 [6], based on instantaneous Navier–Stokes equation. These are finite difference codes based on the porous body approach and solve mass, momentum and energy equations in the orthogonal and rectilinear co-ordinate system. The basic numerical solution techniques for the AQUA and DINUS-3 codes relied on the modified incompressive continuous-fluid Eulerian (MICE) method [7] and the leap-frog method [8], respectively. In these methods, the time step size should be strictly less than that specified by the material Courant limit ($\Delta t_c = \Delta x/u$; Δx is the mesh size and u is the flow velocity). The incomplete Cholesky Conjugate Gradient (ICCG) method [9] was consistently used for matrix inversion throughout the following applications.

These adaptive control systems can also be implemented with other popular algorithms developed to increase the stability of the flow computations, such as the streamline-upwind/Petrov–Galerkin (SUPG) [10], pressure stabilization [11] and pressure-stabilizing/Petrov–Galerkin (PSPG) [12–14] techniques.

2. STRUCTURE OF THE PRESENT CONTROL SYSTEM

A block diagram of the control system is shown in Figure 1. The system consists of three major subsystem blocks around the code: the basic fuzzy controller, the automatic modifier of membership functions and the qualitative inference system based on the fuzzy logic. Very briefly, major functions of these subsystems are to yield an optimum time step size for the next time step; to make judgement on the appropriateness of the new time step given by the basic fuzzy controller; to modify the

DOI: 10.1002/fld

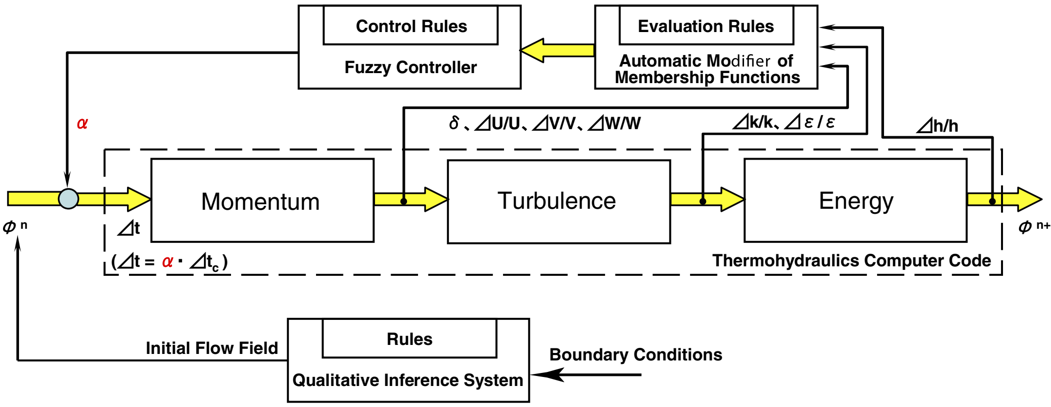

Figure 1. Block diagram of adaptive control system.

membership functions to be used in the basic fuzzy controller; and to give an initial guess to the code with respect to the velocity distribution. Therefore, the qualitative inference is achieved on the off-line system prior to going into the numerical simulation. A more detailed description of these three subsystems is given in the following.

2.1. Basic fuzzy controller

During iterative procedures employed in the code to obtain the converged solution of the three conservation equations per time step, behaviours in the course of numerical integration are monitored by checking the mass residual and relative variations defined as $(\phi^{n+1}-\phi^n)/\phi^n$ every time step, where ϕ represents three velocity components, i.e. u, v and w, k and ε are turbulent parameters in the case of the AQUA numerical simulation, h is enthalpy. $n+1$ indicates the advanced time step and n the present time step. Thereby the optimum value α, the relaxation factor to be multiplied with the critical time step size Δt_{c}, is determined from linguistic rules and membership functions based on the experts' knowledge.

The linguistic rules are represented by five production rules, i.e. by five kinds of 'if and then' logic in the controller. The control strategy is as follows:

(a1) If $(\phi^{n+1}-\phi^n)/\phi^n$ is very large, then apply very small α.
(a2) If $(\phi^{n+1}-\phi^n)/\phi^n$ is large, then apply small α.
(a3) If $(\phi^{n+1}-\phi^n)/\phi^n$ is medium, then keep the present α.
(a4) If $(\phi^{n+1}-\phi^n)/\phi^n$ is small, then apply large α.
(a5) If $(\phi^{n+1}-\phi^n)/\phi^n$ is very small, then apply very large α.

The membership functions were defined corresponding to the above linguistic rules, i.e. five membership functions for five 'if' statements and five membership functions for five 'then' statements. An optimum relaxation factor α is determined along the following sequence.

1. *Input relative variations*. The maximum of $(\phi^{n+1}-\phi^n)/\phi^n$ in all the mesh cells is evaluated for each relevant variable and read by the controller.

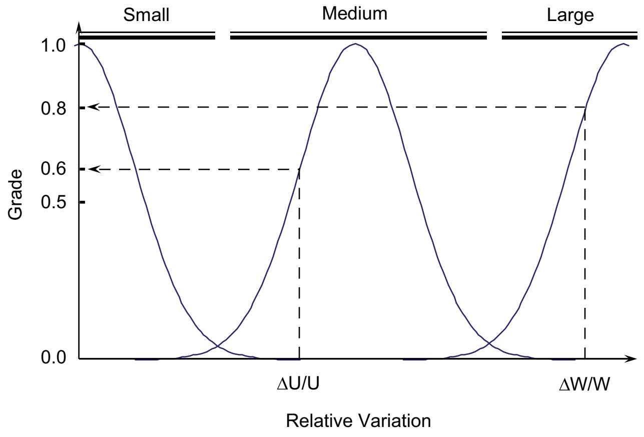

Figure 2. Evaluation of the code condition.

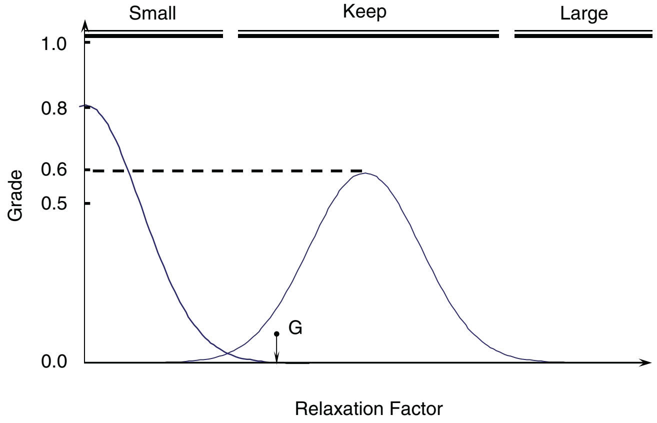

Figure 3. Synthesis of recovery actions.

2. *Evaluate the code condition*. The 'if' statements of the linguistic rules ((a1)–(a5)) are applied to the variations of the state variables ϕ (input) and the membership functions are selected. The membership functions yield a grade of confidence level from 'stable' ($(\phi^{n+1} - \phi^n)/\phi^n$ is small) to 'unstable' ($(\phi^{n+1} - \phi^n)/\phi^n$ is large) for the relative variation (Figure 2, for a two-dimensional problem).
3. *Adjust membership functions in the 'then' statements*. Having obtained the grades for all the relevant variables, the membership functions in the 'then' statement are adjusted by multiplying weighting factors corresponding to the grades to original membership functions (Figure 3).
4. *Deduce recovery actions*. Recovery actions corresponding to each result in step 2 are deduced from the 'then' statement of the linguistic rules ((a1)–(a5)) and the membership functions.

DOI: 10.1002/fld

5. *Synthesize recovery actions*. A centre of gravity of the area, which is a union of the areas surrounded by membership function curves and the abscissa indicating their base set, is calculated (Figure 3). This centre of gravity is projected onto the base set and, as a result, one recovery action from all the recovery actions pertinent to the relative variations is picked up. The recovery action is expressed in terms of the optimum relaxation factor α. Then an actual time step size Δt to be used in the next time step is given by $\alpha\Delta t_{\mathrm{c}}$.

2.2. *Automatic modifier of membership functions*

Consider the situation where the basic fuzzy controller recognized the flow as under forced convection condition while the actual flow is under natural convection condition. In this case, 'numerical experts' try to change the bases of judgement as to the convergence behaviours from that for the forced convection to the natural convection flows. This function was formulated in the system which was referred to as the self-organizing control algorithm suggested by Procyk and Mamdani [15]. The system also has linguistic rules and membership functions to evaluate control performances. The control performances evaluation is carried out using three linguistic rules and three membership functions.

Finally, the positions of membership functions on the base sets in the basic fuzzy controller are tuned in accordance with the control performances evaluation. The linguistic rule is given in the following (also see Figure 4):

(b1) If control performance $(((\phi^i-\phi^{i-1})/(\phi^{i+1}-\phi^i))/\phi^i)\equiv \mathrm{grad}\,\phi)$ is very good ($\mathrm{grad}\,\phi\leqslant -50$), then do not slide the membership function.

(b2) If control performance is good ($-50 < \mathrm{grad}\,\phi < 50$), then slide the membership function by a small amount (3%).

(b3) If control performance is bad ($\mathrm{grad}\,\phi\geqslant 50$), then slide the membership function by a large amount (5%).

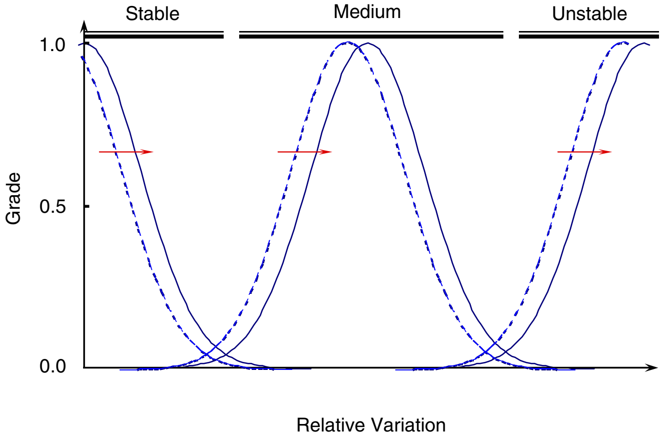

Figure 4. Modification of membership functions.

DOI: 10.1002/fld

The evaluation of the control performances conforms to the following algorithm:

```
1. Input relative variations
   (the same as in the basic fuzzy controller)
2. Deduce the recovery action
   For the same time step, a relaxation factor $a$ is deduced by the basic fuzzy control algorithm
   described in Section 2.1.
3. Evaluate the control performances
   Evaluation of the control performances is made along the following sequence:
      If a control performance is very good,
         go to 4
      Else
         Slide the membership function for the 'if' statements used in the basic fuzzy controller
         on the base set ((a1)–(a5)). The amount of sliding is determined by the above linguistic
         rules ((b1)–(b3)) and membership functions (Figure 4). Its range is 0–5% of the axis
         length of the base set for the relative variations.
      Endif
         go to 2
4. End
```

2.3. *Qualitative inference with the fuzzy logic*

A qualitative inference technique based on the fuzzy logic was formulated in the system and employed in order to guess an initial velocity field in any flow geometry. This initial guess is useful in reducing the total CPU time to reach a steady-state condition. Therefore, code users are not required to have a deep knowledge of the numerical methods and thermohydraulics in order to set up an initial flow distribution. The initial velocity field is deduced using 'common-sense knowledge' on hydrodynamics. The 'common-sense knowledge' used here is given in the following, for example:

(1) Fluid flows from inlet to outlet.
(2) Fluid flows along solid wall.
(3) Normal velocity to the solid wall is zero.
(4) Momentum changes its direction in the presence of obstacles in the downstream direction.

The knowledge (4) above is modified by the fuzzy logic to rectify abrupt changes of the flow directions. For example, the momentum direction is determined in consideration of the effect of the distance from the solid wall. In this work, also the effect of friction force from the solid wall is accounted. The linguistic rule is given in the following:

(c1) If the distance to the solid wall is small, then its effect is large.
(c2) If the distance to the solid wall is medium, then its effect is medium.
(c3) If the distance to the solid wall is large, then its effect is small.

The qualitative inference is carried out through the following algorithm:

1. Input the boundary condition.
   The distances from all the cell surfaces to solid walls are read by the system for all the cells.
2. Infer the magnitude of velocity vector.

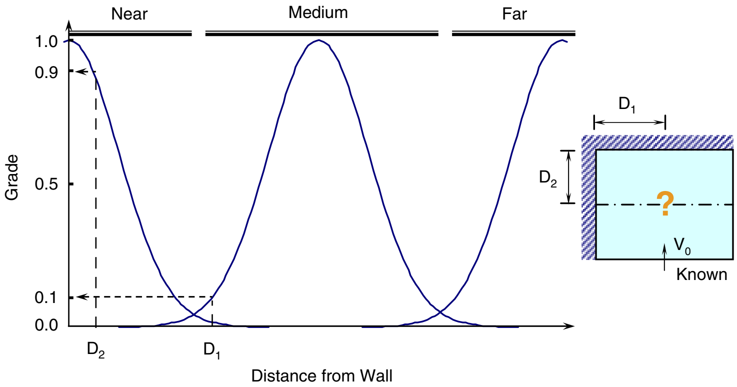

Figure 5. Evaluation of wall effects.

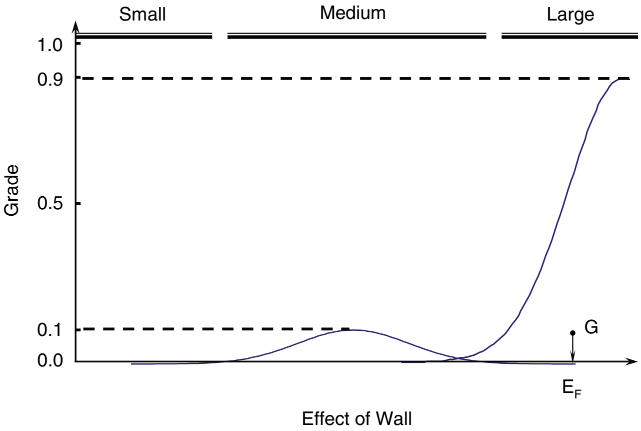

Figure 6. Synthesis of wall effects.

A magnitude of the flow velocity component on each cell surface is inferred using the fuzzy logic consistent with the linguistic rules ((c1)–(c3)) and the membership functions based on the 'common-sense knowledge' (Figures 5 and 6). At this step, the mass continuity must always be conserved.

3. Synthesize velocity vector components.
   The velocity vector for the cell is determined by the information obtained in step 2.

3. NUMERICAL EXPERIMENTS FOR STEADY-STATE FLOWS

3.1. Outline of the calculations

An *r–z* two-dimensional mesh arrangement (38 × 44) is shown in Figure 7. Non-structured cells, which are defined as those without solid structure inside the cell, count up to 1188. It represents

DOI: 10.1002/fld

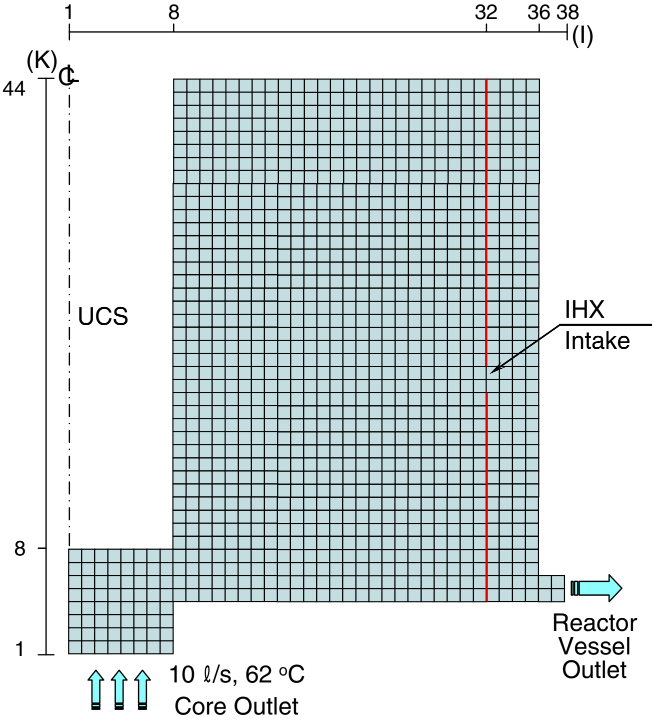

Figure 7. Mesh arrangement for hot plenum of LMFBR.

an experimental apparatus simulating a hot plenum of pool-type LMFBRs. Water was used as a working fluid instead of sodium. A no-slip condition for velocity components and an adiabatic condition were applied on the solid surfaces. As the initial steady-state conditions, the isothermal stagnant water (62°C) was filled in the plenum. Then the inlet flow rate was suddenly increased from zero to 16 l/s. Transient calculations were continued until the steady-state conditions were reached. In the calculation with the AQUA code, convective terms in the conservation equations were dealt with by QUICK for the momentum flux, QUICK-FRAM for the energy flux and the first-order upwind scheme for the turbulence quantities.

3.2. Survey of the membership functions

Before the comparison with the results when the control system was not used, effects of the profile and the number of membership functions were investigated. Membership functions with Gaussian, triangle and trapezoid profiles were chosen. On the other hand, three, five and seven membership functions were selected. The calculations were carried out for a total of nine cases (Runs A-1 to A-9) indicated in Table I. In the calculations, the automatic modifier of the membership functions and the qualitative inference system were not used to confirm solely the effects of the membership functions on the control performance. Figure 8 shows each membership function for the 'if' statements and the 'then' statements considered here.

DOI: 10.1002/fld

Table I. Calculational cases for survey of membership functions.

	Number of membership functions		
Profile of membership function	3	5	7
Gaussian	Run A-1	Run A-2	Run A-3
Triangle	Run A-4	Run A-5	Run A-6
Gaussian	Run A-7	Run A-8	Run A-9

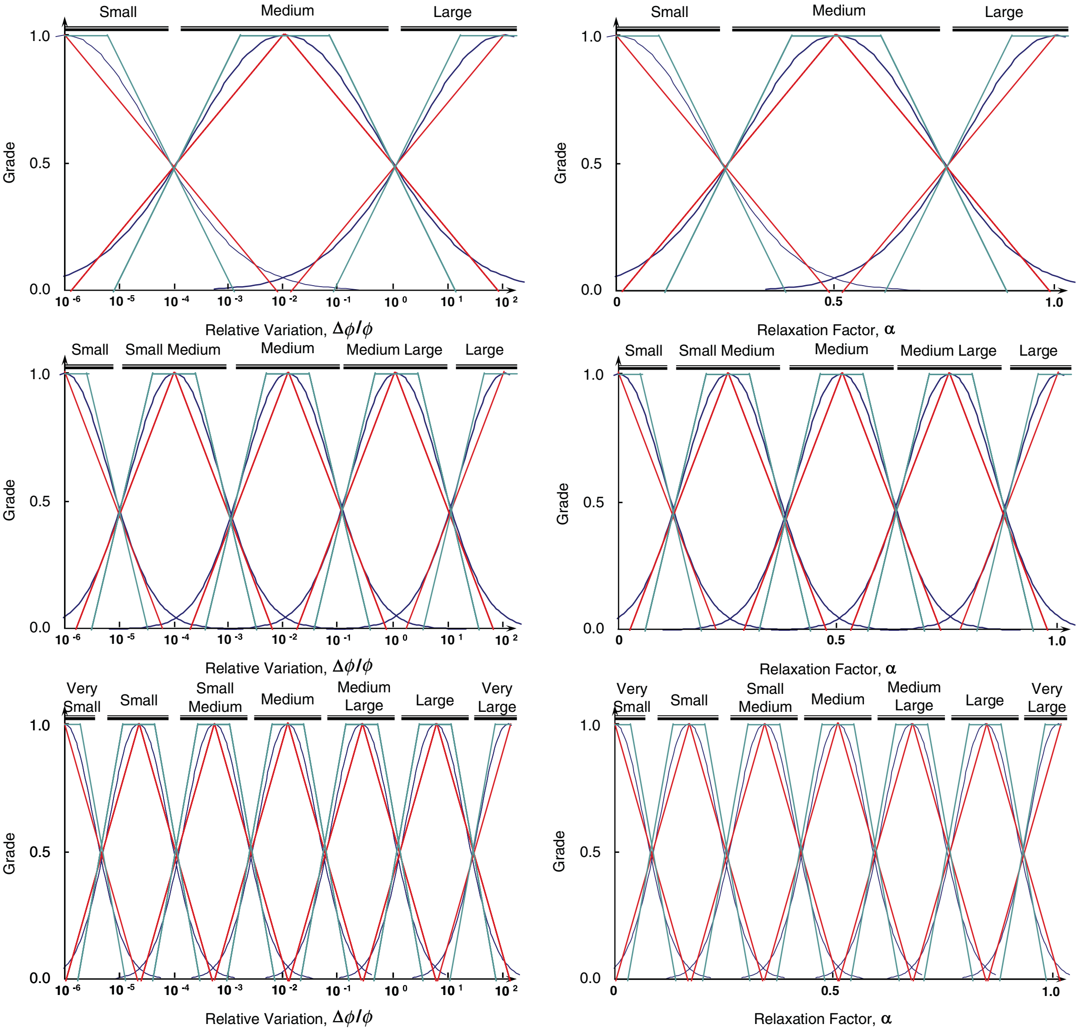

Figure 8. Membership functions for ‘if and then’ statements.

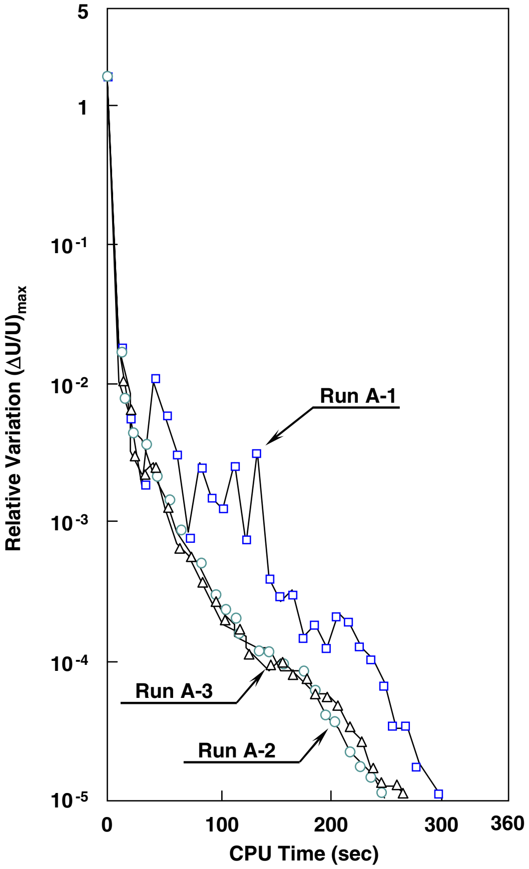

Figure 9. Effect of number of membership functions on convergence using the Gaussian profile (Runs A-1–A-3).

Figures 9–11 show convergence curves for the nine cases to a steady-state condition in terms of relative variation of the velocity component u as a representative and CPU time consumption. The variable u was selected since its relative variation took maximum effort in reaching the convergence. Here a convergence is judged to be attained when the relative variations are less than 10^{-5}.

Calculations using the Gaussian profile as the membership functions (Figure 9) showed that a relatively large numerical instability appeared in the Run A-1 calculation compared to that in Runs A-2 and A-3. One of the reasons is that the control characteristics are rougher for Run A-1 than for Runs A-2 and A-3 due to fewer membership functions. On the other hand, from the comparison of Runs A-2 and A-3, it was confirmed that the control performance was saturated with five membership functions. As for the results of Runs A-4 to A-9 (Figures 10 and 11), using the triangle and the trapezoid profiles, these gave characteristics similar to Runs A-1 to A-3 using the Gaussian profile.

DOI: 10.1002/fld

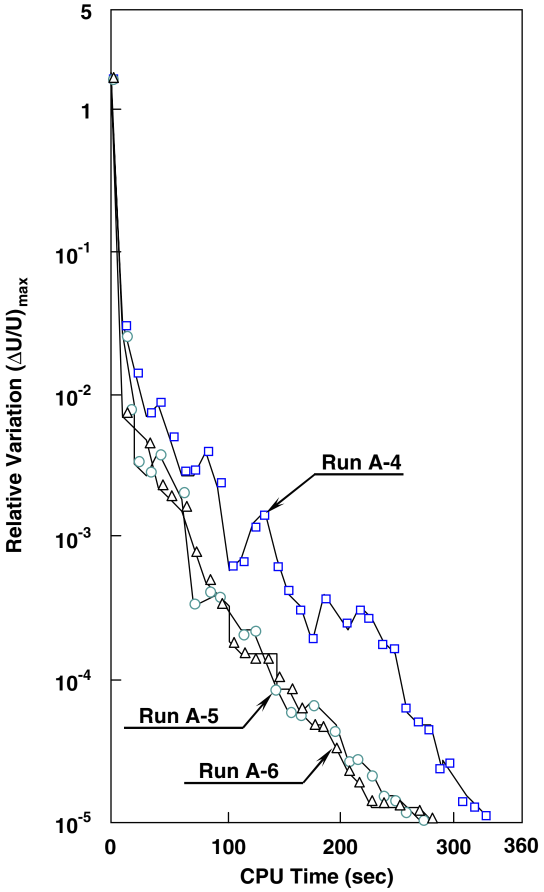

Figure 10. Effect of number of membership functions on convergence using the triangle profile (Runs A-4–A-6).

Figure 12 shows a comparison of the convergence curves for various profiles using five membership functions, indicating that there is no significant difference among Runs A-2, A-5 and A-8.

The above results indicated that the control performance depended on the number of membership functions rather than on the profile of the functions. For the following calculations, a combination of five membership functions using the Gaussian profile was employed as a standard method.

3.3. Performance of the control system

The calculations using the constant relaxation factor α were carried out for a total of four cases (Runs B-1 to B-4). The relaxation factor α for these cases was set as 0.8, 0.5, 0.3 and 0.1, respectively. On the other hand, the calculations using the adaptive control system were carried out for three cases (Runs A-2, A-2A and A-2B). Run A-2 is the result indicated in the previous section. Runs A-2A and A-2B are results obtained by the adaptive control system with the automatic modifier

DOI: 10.1002/fld

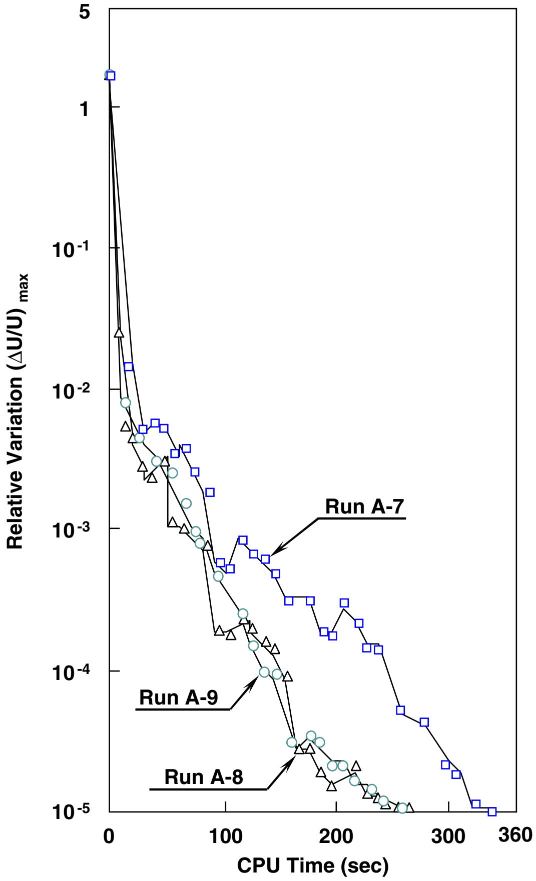

Figure 11. Effect of number of membership functions on convergence using the trapezoid profile (Runs A-7–A-9).

of the membership functions and the qualitative inference system, respectively. Figure 13 shows convergence curves for the six cases to the steady-state condition.

In the calculations of Runs B-1 and B-2, on the one hand, large numerical instabilities were observed due to large time step sizes throughout. As a result, the calculations did not indicate the convergence to a steady state for the CPU time specified in the figure. On the other hand, in the results from Runs B-3 and B-4, the numerical instabilities were less dominant than those of B-1 and B-2. However, for both B-3 and B-4 curves, the numerical instability is observed for a long time on the order of 10^{-4}. The results with the adaptive control system (Runs A-2 and A-2A) show good convergence characteristics in comparison with those of the above four cases. Especially, the slope of Run A-2A was steeper than that of Run A-2.

Figure 14 shows the histories of the relaxation factor α when the time step size was controlled by the system (Runs A-2 and A-2A). Both were decreased rapidly from a default value (0.8) to a value in the neighbourhood of 0.2 upon starting the calculation, and then slowly increased until the steady-state condition was reached. The main difference between the two is a reversal of the

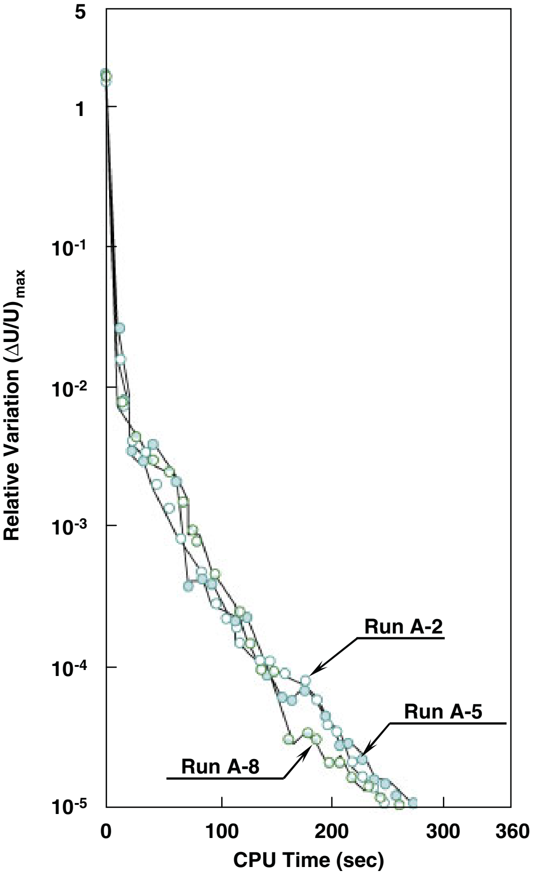

Figure 12. Effect of profile of membership functions on convergence under three 'if and then' statements.

α value at 60 s. In the result of Run A-2A, α of an initial stage of 60 s is smaller than that of the Run A-2 calculation; then the tendency changes at the later stage (> 60 s).

Figure 15 shows a comparison of the steady-state velocity distributions in the experimental and numerical results from the AQUA code with the controller and from the qualitative inference. The result obtained using the qualitative inference system, which was in fact used as the initial condition for the velocity distribution calculation by the AQUA code, gave a trend of the flow pattern similar to both the experimental and the numerical results except for the direction and intensity of a jet into the plenum from the inlet (the subassembly outlet; see Figure 7). It should be noted that the qualitative inference system will produce the same flow pattern regardless of the different inlet mass flow rates. As shown in Figure 15, the velocity distribution calculated by the AQUA code was in good arrangement with that of experiment which had been obtained by a small propeller velocimeter [16]. We note here that the arrangement was due mostly to the incorporation of the difference method of higher-order accuracy in space for convection terms and was not influenced by the introduction of the adaptive time step size controller.

DOI: 10.1002/fld

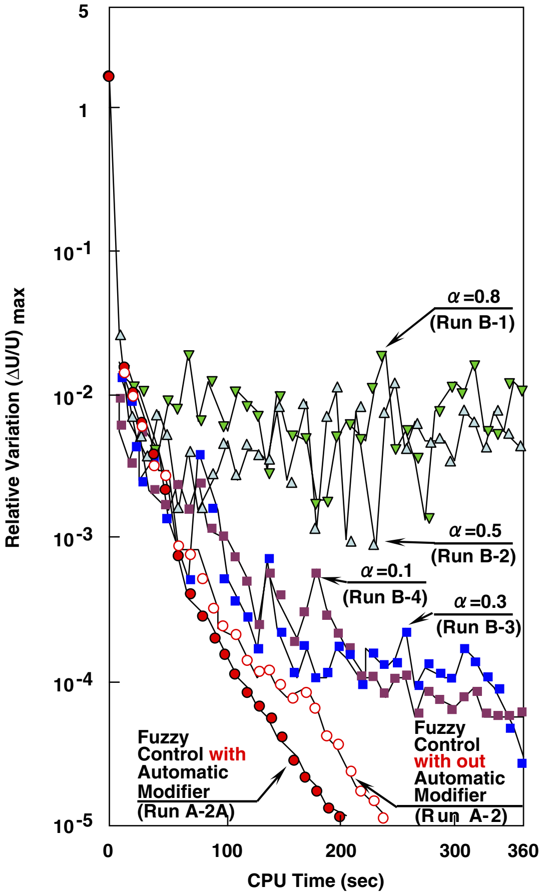

Figure 13. Comparison of convergence curves to steady-state level.

Figure 16 illustrates the relationship between the total CPU time to a steady-state level $(\Delta u/u)_{\max} = 10^{-5}$ and the relaxation factor α. Symbol '$\circ$' denotes the results when the adaptive control system was not used and α was kept constant. It is noted, in this case, that there is an optimum relaxation factor unique to the AQUA code, of course, and will vary depending on the problems to be solved. In the result obtained by the adaptive control system, it was found that the total CPU time to a steady-state level was reduced typically to 50% compared to that of the optimum case (Run B-3 with $\alpha = 0.3$). Further, the additional use of an initial guess for the velocity distribution, which was obtained by the qualitative inference system, reduced the total CPU time to about 40% as compared to the Run B-3 calculations starting from the stagnant water at the beginning.

The above results indicated that the optimum relaxation factor α in the course of numerical integration changed from time to time: α was determined effectively by the adaptive control system based on the fuzzy theory.

DOI: 10.1002/fld

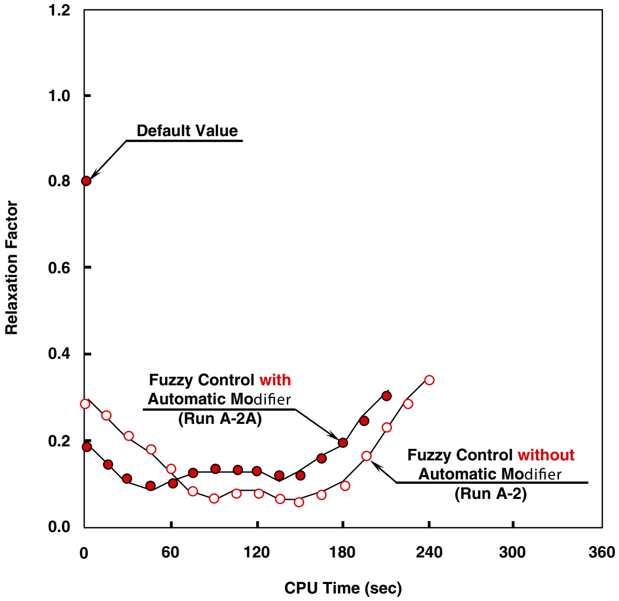

Figure 14. Time histories of relaxation factor α.

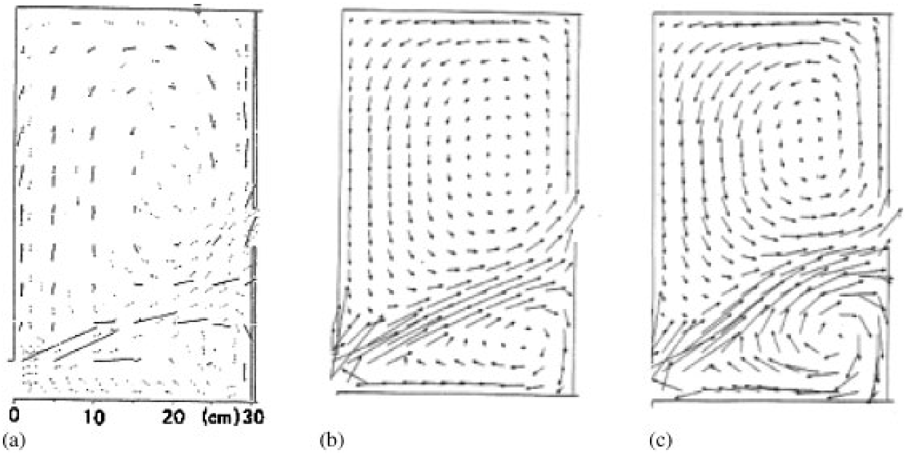

Figure 15. Comparison of velocity distribution between numerical and qualitative inference solutions: (a) experiment; (b) numerical solution; and (c) qualitative inference solution.

4. NUMERICAL EXPERIMENTS FOR TRANSIENT FLOWS

4.1. Outline of the calculation

In this section, an application of the adaptive control system is made to a transient experiment carried out on the same system as described in the previous section. As the initial condition, the

DOI: 10.1002/fld

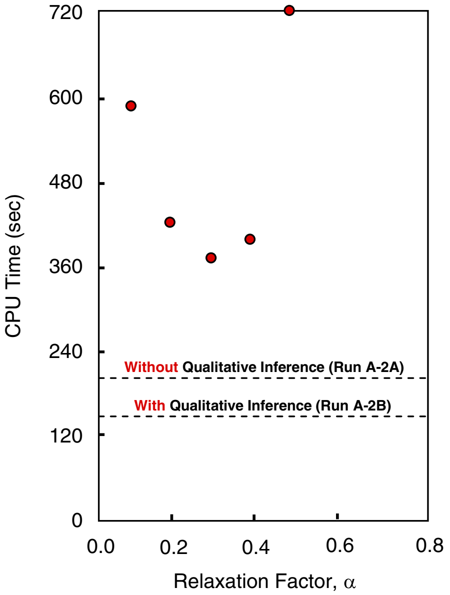

Figure 16. α dependence of total CPU time to steady-state level.

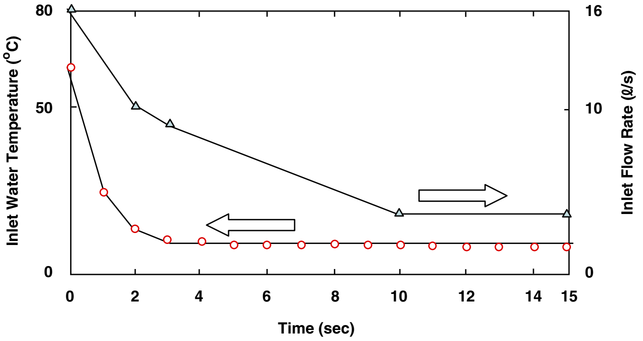

Figure 17. Temperature and mass flow rate transients at the inlet position.

steady-state isothermal flow field obtained in the previous section was used in the hot plenum before going into transients. In the transient experiment, the water temperature at the inlet was changed from 62 to 9.6°C in 30 s and the inlet mass flow rate from 16 to 3.84 l/s in 10 s. Then the inlet mass flow rate and the temperature were kept constant (see Figure 17). Two transient calculations were carried out to simulate the experiment with the same higher-order treatment of the convection terms as used in Section 3.1: i.e. one by the use of the constant relaxation factor $\alpha = 0.2$ (Run C-1) and the other by the use of the adaptive control system (Run C-2). The membership functions were the same as those described in Section 3.2.

DOI: 10.1002/fld

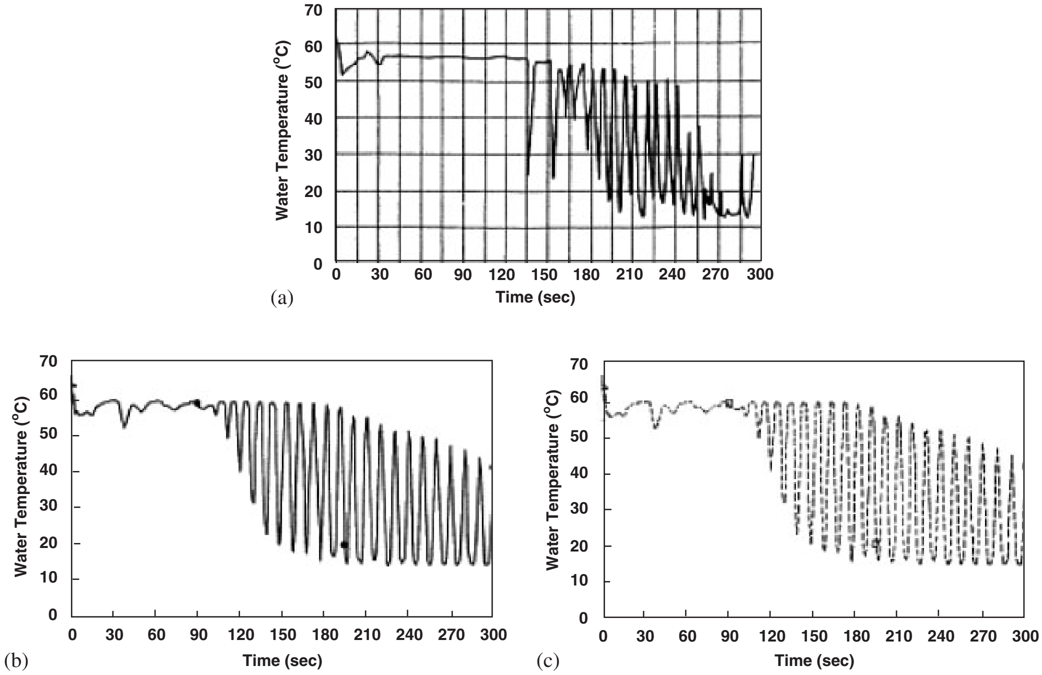

Figure 18. Comparison of temperature histories in the hot plenum: (a) experiment; (b) Run C-1 ($\alpha = 0.2$); and (c) Run C-2 (fuzzy control with automatic modifier).

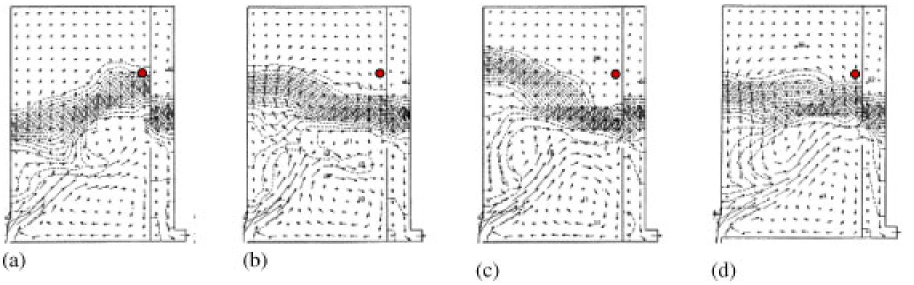

Figure 19. Calculated temperature and velocity vector fields: (a) $t = 150$ s; (b) $t = 152$ s; (c) $t = 154$ s; and (d) $t = 156$ s.

4.2. Results and discussions

Figure 18 compares typical temperature histories among (a) the experiment, (b) Run C-1 and (c) Run C-2 at the location x ($I = 32$ and $K = 30$) as shown in Figure 7. It is noted that Runs C-1 and C-2 gave exactly the same temperature histories (Figure 18(b) and (c)). As shown in the figure, a continuous temperature oscillation observed in the experiment (Figure 18(a)) was predicted well by both the calculations. The temperature oscillation was due to an internal sloshing behaviour of the thermal stratification interface, i.e. as shown in Figure 19 (by Run C-2). Furthermore, there

DOI: 10.1002/fld

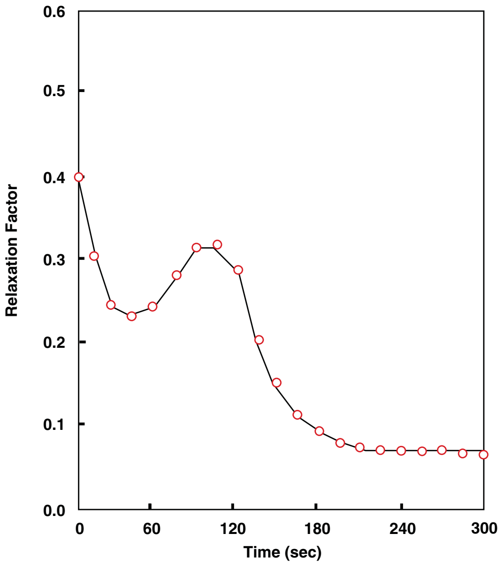

Figure 20. Time history of relaxation factor α.

is no difference in the temperature histories between Runs C-1 and C-2. From these results, it is considered that the time step sizes determined by the adaptive control system did not directly affect the computational results.

Figure 20 shows a history of the relaxation factor α determined by the control system. The α value was reduced from a default value of the transient case (0.4) to a value in the neighbourhood of 0.2 upon starting the calculation (−60 s), and then slowly increased to 0.3 (−100 s). However, the α value was reduced to 0.1 when the internal sloshing behaviour was calculated (> 100 s).

Figure 21 compares the relationship of accumulated CPU time and simulation time to 300 s between Runs C-1 and C-2. Symbol '□' denotes the results of Run C-1 ($\alpha = 0.2$). In this case, the accumulated CPU time increased linearly with the simulation time. In the result obtained by the adaptive control (Run C-2; symbol '○'), it was found that the accumulated CPU time to the 300 s simulation was reduced to about 65% as compared to that of Run C-1 ($\alpha = 0.2$). Note that the gradient of the Run C-2 curve is slightly less than that of the Run C-1 curve even after the α value was set smaller than 0.2. This is due to the fact that much fewer iterations were required for each time step than when $\alpha = 0.2$.

From the above results, it is concluded that the adaptive control system has a potential to save computing efforts for thermohydraulic transient calculations.

5. LARGE-SCALE NUMERICAL SIMULATIONS

5.1. Outline of a large-scale steady-state calculation

The adaptive control system was applied to a three-dimensional in-vessel thermohydraulics calculation of a typical loop-type LMFBR generating 714 MW thermal output as a large-scale steady-state

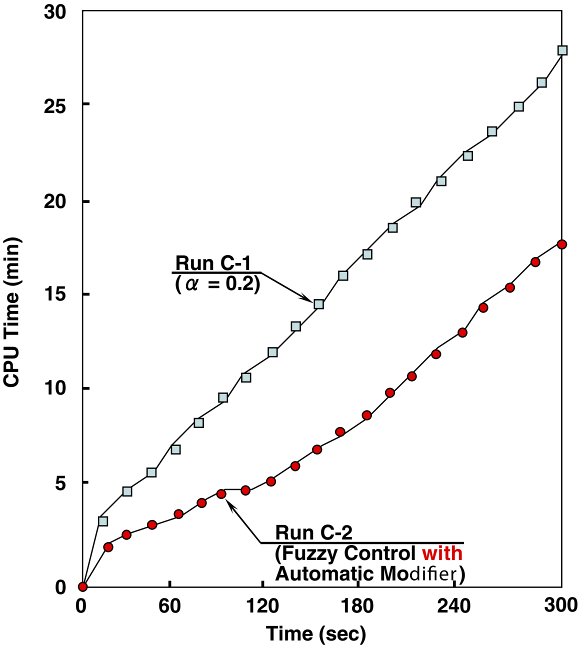

Figure 21. Relationship of accumulated CPU time and simulation time.

problem. Figure 22 shows a cut-view of the reactor. The reactor vessel contains the core, internal structure, upper core structure and inner barrel.

In the present analysis, calculations with the AQUA code were carried out for a $\frac{1}{3}$ sector of the reactor vessel assuming a 120° symmetry. Figure 23 illustrates the three-dimensional mesh arrangement (r–θ–z) with 26 496 mesh points ($= 32 \times 12 \times 69$), out of which 23 270 are non-structured cells. Here the 'non-structured cell' is defined as a computational cell which contains no solid structure inside. Time-marching transient calculations were continued until the steady-state condition for a full-power operation condition of the plant was reached. As for calculational schemes of the convective terms, a combination identical to the one used in the numerical experiments analysis was employed.

5.2. Results and discussions on the steady-state calculation

The steady-state calculations were carried out for two cases by the use of the constant relaxation factor $\alpha = 0.3$ and the adaptive control system. The two calculations gave an identical result for the velocity and temperature distributions of the steady state. The calculated distributions are shown elsewhere, for example, in Reference [17]. Figure 24 shows convergence curves for the two cases to the steady-state condition. The numerical instability of the result obtained by using constant α was small; however, the curve stayed, for a long time, around 3×10^{-5}. On the other hand, the result with the adaptive control system indicates good convergence characteristics as compared to the above case. From the above results, it was found that the total CPU time to a steady-state level was reduced to about 25% compared to that without the adaptive control of the time step sizes.

DOI: 10.1002/fld

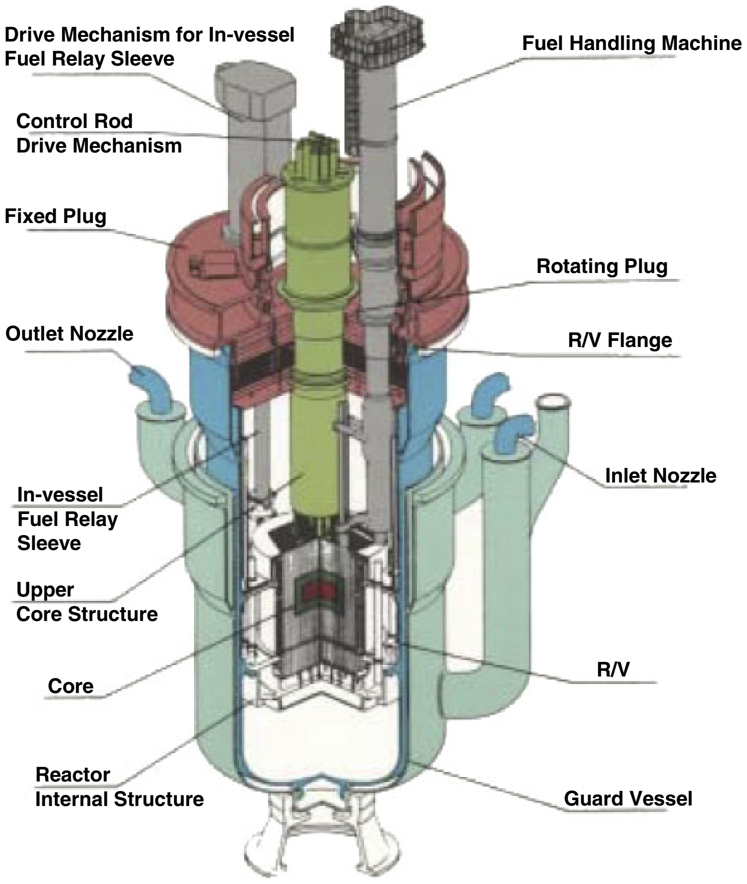
Drive Mechanism for In-vessel Fuel Relay Sleeve
Control Rod Drive Mechanism
Fixed Plug
Outlet Nozzle
In-vessel Fuel Relay Sleeve
Upper Core Structure
Core
Reactor Internal Structure
Fuel Handling Machine
Rotating Plug
R/V Flange
Inlet Nozzle
R/V
Guard Vessel

Figure 22. Cut-view of a prototype LMFBR system.

Figure 25 shows a history of the relaxation factor α determined by the control system. The results gave a tendency similar to the numerical experiments analysis indicated in Figure 16. The α value decreased rapidly from the default value to 0.15 on starting the calculation, and then slowly increased until the steady-state condition was reached.

5.3. Outline of a large-scale transient calculation

The adaptive control system was applied to a three-dimensional fluid–structure thermal interaction calculation in a T-junction piping system as a large-scale multi-physics transient problem. Figure 26 illustrates geometrical characteristics of the piping system in a French LMFBR Phenix. The main pipe in the T-junction area consists of a horizontal straight part, a 90° elbow and a vertical straight pipe, where the T-junction is connected. A circumferential weld is located at 160 mm downstream position from the T-junction in the vertical straight part of the main pipe. Some earlier FSI work also targeted fluid mechanics problems involving pipes, see, for example, Reference [18].

DOI: 10.1002/fld

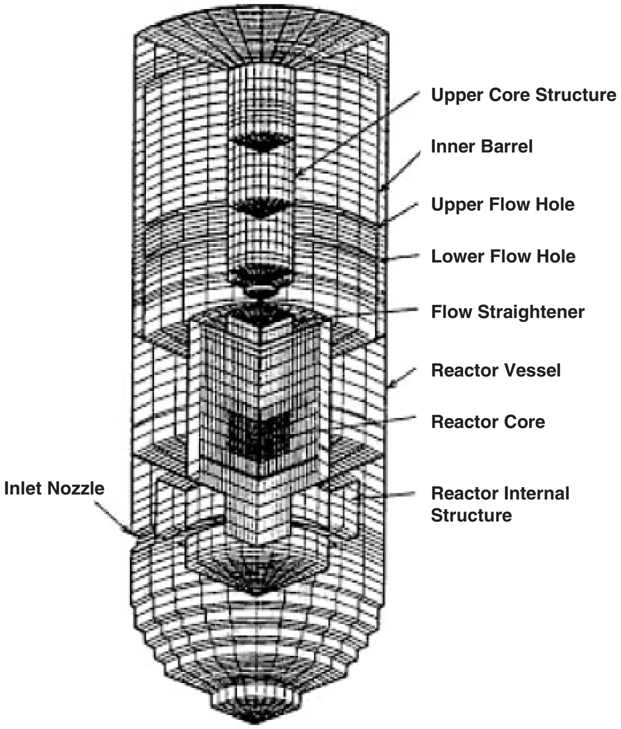

Figure 23. Mesh arrangement of the reactor vessel.

In this analysis, fluid–structure thermal interaction calculations with the DINUS-3 code were carried out for a partial domain of the vertical straight pipe including the T-junction. Figure 27 shows the three-dimensional mesh arrangement (r–θ–z) with 177 570 mesh points ($22 \times 77 \times 115$). Transient calculations from a thermohydraulics quasi-steady-state condition were carried out for 10s simulation time. In the calculations, a combination of the modified third-order upwind scheme for the convection term and the leap-frog time integration scheme was used. The fluid–structure thermal interaction model used in the calculation is shown in Reference [19]. There are various ways of solving the coupled fluid and structural mechanics equations (see, for example, References [20, 21]). In our computations we are solving the coupled equations with a block-iterative coupling technique.

5.4. Results and discussions on the transient calculation

A transient calculation was carried out for one case only with the adaptive control system. Figure 28 shows a calculated instantaneous sodium temperature distribution at 0.1 mm from the main pipe inner surface. As shown in the figure, thermal fluctuations were evaluated due to turbulence interactions between both the jets from the main and the branch pipes without any numerical instability. Furthermore, cracked positions evaluated by a fracture mechanics code using the time series data from the fluid–structure thermal interaction calculations agreed well with actual positions shown in Figure 29.

DOI: 10.1002/fld

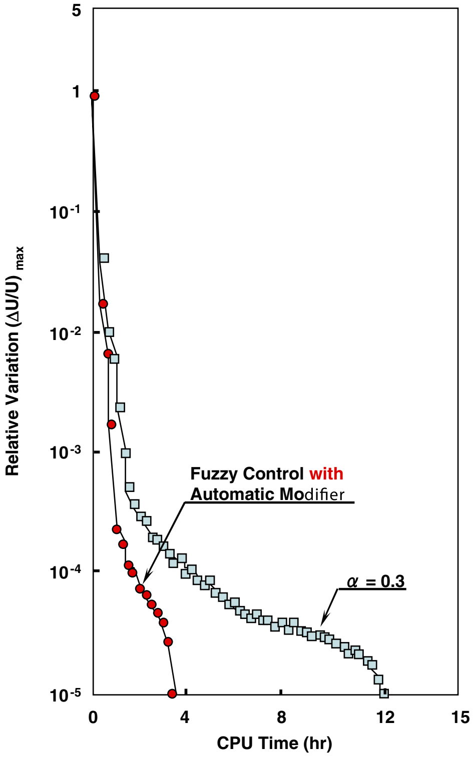

Figure 24. Comparison of convergence characteristics to steady-state level.

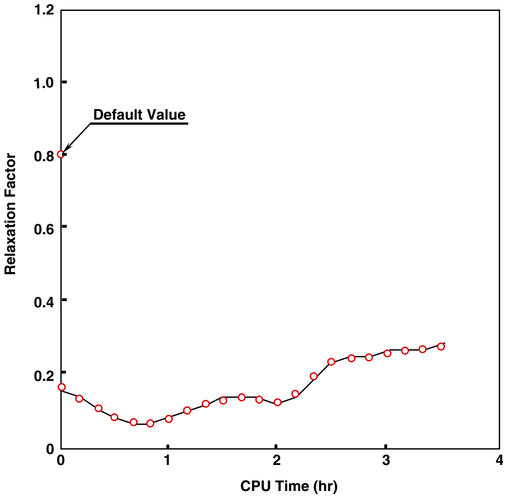

Figure 25. Time history of relaxation factor α.

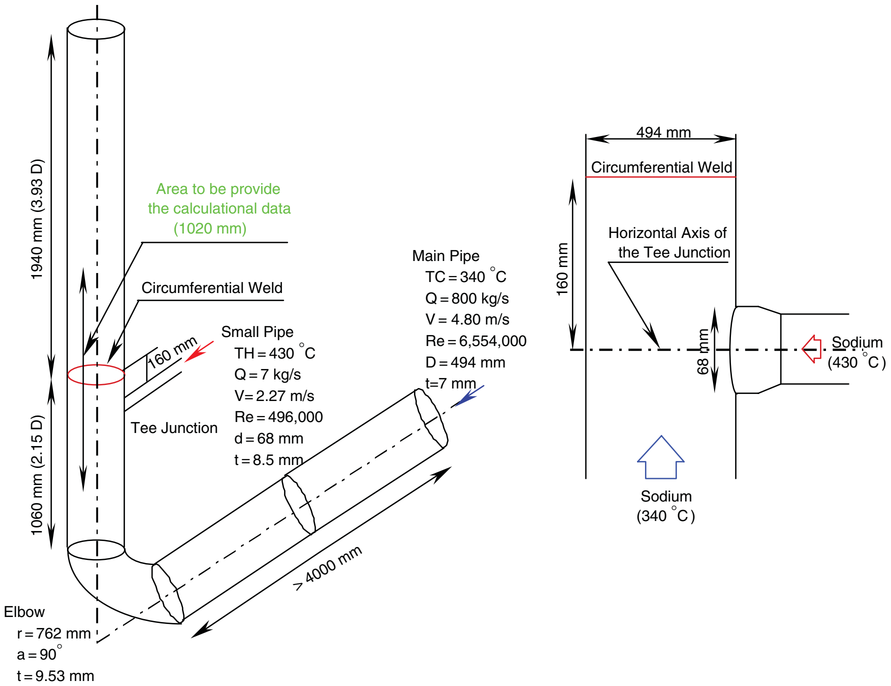

Figure 26. Geometrical characteristics of a T-junction piping system in French LMFBR Phenix.

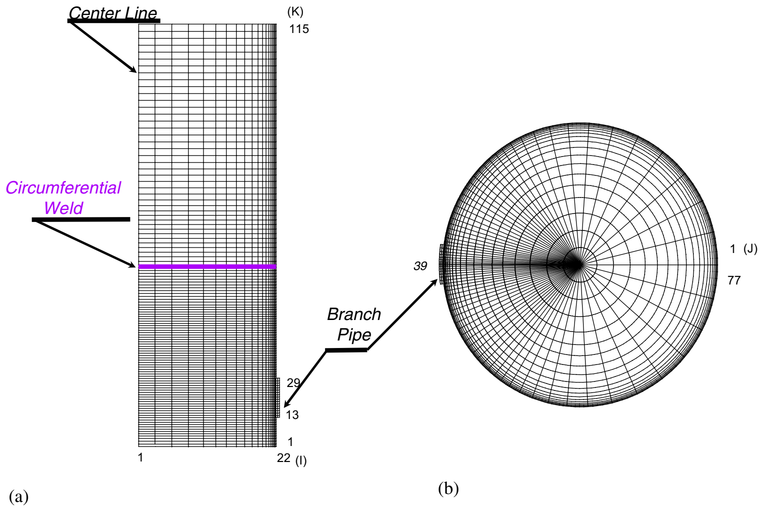

Figure 27. Mesh arrangement for the T-junction piping system: (a) r–z plane and (b) r–θ plane.

DOI: 10.1002/fld

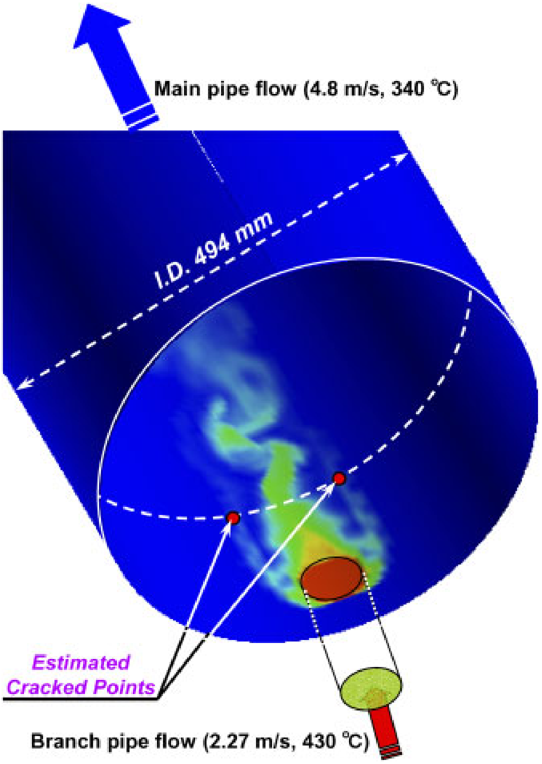

Figure 28. Calculated instantaneous sodium temperature distribution.

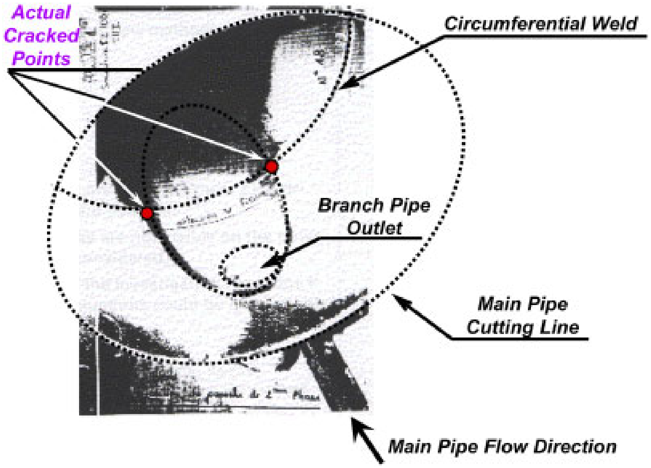

Figure 29. Cracking positions observed in the Phenix reactor.

DOI: 10.1002/fld

6. CONCLUSIONS

The adaptive control system was developed in an attempt to yield the optimum time step sizes using the fuzzy theory for the transient multi-physics numerical simulation code. The system aimed at eliminating numerical instabilities which were often encountered during transient calculations with higher-order accuracy numerical schemes and eventually at reducing the computing cost. It was implemented into the AQUA and DINUS-3 codes and was successfully applied to a sample problem and to realistically large-scale problems. Calculations of the sample problem with the use of the adaptive control system showed less than 50% of the computing time required when the time step size was not controlled by the system. In the calculations of the large-scale steady-state problem, total CPU time to attain the steady-state was reduced to about 25% compared to that for the case with constant relaxation factor $\alpha = 0.3$. In the large-scale multi-physics transient problem, physical thermal fluctuations were calculated without any numerical instability. The result obtained in this work is very encouraging: the adaptive control system would be one of the efficient measures to save computing efforts when one wishes to perform extremely large-scale simulation of the transient multi-physics problem of long time duration.

REFERENCES

1. Leonard BP. A stable and accurate convective modeling procedure based on quadratic upstream interpolation. *Computer Methods in Applied Mechanics and Engineering* 1976; **9**.
2. Chapman M. FRAM—nonlinear damping algorithms for the continuity equation. *Journal of Computational Physics* 1984; **44**.
3. Zadeh LA. Fuzzy algorithms. *Information and Control* 1968; **12**.
4. Yagawa G (ed.). *Application of Fuzzy Logic to Computational Mechanics and CAE*. Baifukan: Tokyo, 1991.
5. Maekawa I, Muramatsu T. Higher order difference schemes and their applications to in-vessel thermal-hydraulic analysis. *Proceedings of the Fifth IAHR Liquid Metal Working Group Meeting*, Grenoble, France, 1986.
6. Muramatsu T. Numerical analysis of nonstationary thermal response characteristics for a fluid–structure interaction system. *Journal of Pressure Vessel Technology* 1999; **121**.
7. Harlow FH, Amsden AA. A numerical fluid dynamics calculation method for all flow speeds. *Journal of Computational Physics* 1971; **8**.
8. Roache PJ. *Computational Fluid Dynamics*. Helmosa, 1976.
9. Meijerink JA, Van Der Vorst. An iterative solution method for linear systems of which the coefficient matrix is a symmetric M-matrix. *Mathematics of Computation* 1977; **31**.
10. Brooks AN, Hughes TJR. Streamline Upwind/Petrov–Galerkin formulations for convection dominated flows with particular emphasis on the incompressible Navier–Stokes equations. *Computer Methods in Applied Mechanics and Engineering* 1982; **32**:199–259.
11. Hughes TJR, Franca LP, Balestra M. A new finite element formulation for computational fluid dynamics: V. Circumventing the Babuvska–Brezzi condition: a stable Petrov–Galerkin formulation of the Stokes problem accommodating equal-order interpolations. *Computer Methods in Applied Mechanics and Engineering* 1986; **59**:85–99.
12. Tezduyar TE. Stabilized finite element formulations for incompressible flow computations. *Advances in Applied Mechanics* 1992; **28**:1–44.
13. Tezduyar TE, Mittal S, Ray SE, Shih R. Incompressible flow computations with stabilized bilinear and linear equal-order-interpolation velocity-pressure elements. *Computer Methods in Applied Mechanics and Engineering* 1992; **95**:221–242.
14. Tezduyar TE. Computation of moving boundaries and interfaces and stabilization parameters. *International Journal for Numerical Methods in Fluids* 2003; **43**:555–575.
15. Procyk TJ, Mamdani EM. A linguistic self-organizing process controller. *Automatica* 1979; **15**.
16. Tanaka N, Moriya S, Fujimoto K. Thermal hydraulic characteristics in reactor vessel of pool-type fast breeder reactor. *Proceedings of the Second International Topical Meeting on Nuclear Power Plant Thermal Hydraulics and Operations*, Tokyo, Japan, 1986.

DOI: 10.1002/fld

17. Ninokata H, Izumi A. Decay heat removal system of the Monju reactor plant and studies related to the passive actuation and performances. *Proceedings of the International Fast Reactor Safety Meeting*, Snowbird, U.S.A., 1990.
18. Mittal S, Tezduyar TE. Parallel finite element simulation of 3D incompressible flows—fluid–structure interactions. *International Journal for Numerical Methods in Fluids* 1995; **21**:933–953.
19. Muramatsu T. Numerical simulation of non-stationary heat transfer process related to thermal striping phenomena. *Proceedings of the ASME/JSME Pressure Vessels and Piping Conference*, San Diego, CA, U.S.A., vol. 458, 2004.
20. Tezduyar TE, Sathe S, Keedy R, Stein K. Space-time finite element techniques for computation of fluid–structure interactions. *Computer Methods in Applied Mechanics and Engineering* 2006; **195**:2002–2027.
21. Tezduyar TE, Sathe S, Stein K. Solution techniques for the fully-discretized equations in computation of fluid–structure interactions with the space-time formulations. *Computer Methods in Applied Mechanics and Engineering* 2006; **195**:5743–5753.